

MIT Open Access Articles

The Global Color of Pluto from New Horizons

The MIT Faculty has made this article openly available. **Please share** how this access benefits you. Your story matters.

Citation: Olkin, Catherine B. et al. "The Global Color of Pluto from New Horizons." *The Astronomical Journal* 154, 6 (November 2017): 258 © 2017 The American Astronomical Society

As Published: <http://dx.doi.org/10.3847/1538-3881/AA965B>

Publisher: American Astronomical Society

Persistent URL: <http://hdl.handle.net/1721.1/117559>

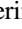





Version: Final published version: final published article, as it appeared in a journal, conference proceedings, or other formally published context

Terms of Use: Article is made available in accordance with the publisher's policy and may be subject to US copyright law. Please refer to the publisher's site for terms of use.





The Global Color of Pluto from New Horizons

Catherine B. Olkin¹ , John R. Spencer¹, William M. Grundy², Alex H. Parker¹ , Ross A. Beyer^{3,4}, Paul M. Schenk⁵, Carly J. A. Howett¹, S. Alan Stern¹, Dennis C. Reuter⁶, Harold A. Weaver⁷ , Leslie A. Young¹, Kimberly Ennico⁴ , Richard P. Binzel⁸, Marc W. Buie¹ , Jason C. Cook⁹, Dale P. Cruikshank⁴, Cristina M. Dalle Ore⁴, Alissa M. Earle⁸, Donald E. Jennings⁶, Kelsi N. Singer¹ , Ivan E. Linscott¹⁰, Allen W. Lunsford⁶, Silvia Protopapa¹¹, Bernard Schmitt¹², Eddie Weigle¹³

and the New Horizons Science Team

¹ Southwest Research Institute, Boulder, CO 80302, USA

² Lowell Observatory, 1400 W Mars Hill Road, Flagstaff, AZ 86001, USA

³ The SETI Institute, Mountain View, CA 94043, USA

⁴ NASA Ames Research Center, Moffett Boulevard, Moffett Field, CA 94035, USA

⁵ Lunar and Planetary Institute, Houston, TX 77058, USA

⁶ NASA Goddard Spaceflight Center, 8800 Greenbelt Road, Greenbelt, MD 20771, USA

⁷ The Johns Hopkins University Applied Physics Laboratory, 11100 Johns Hopkins Road, Laurel, MD 20723, USA

⁸ Massachusetts Institute of Technology, 77 Massachusetts Avenue, Cambridge, MA 02139, USA

⁹ Pinhead Institute, Telluride, CO 81435, USA

¹⁰ Stanford University, 450 Serra Mall, Stanford, CA 94305, USA

¹¹ University of Maryland, College Park, MD 20742, USA

¹² Université Grenoble Alpes, CNRS, IPAG, F-38000 Grenoble, France

¹³ Big Head Endian, Winfield, KS 67156, USA

Received 2017 September 14; revised 2017 October 23; accepted 2017 October 24; published 2017 November 29

Abstract

The New Horizons flyby provided the first high-resolution color maps of Pluto. We present here, for the first time, an analysis of the color of the entire sunlit surface of Pluto and the first quantitative analysis of color and elevation on the encounter hemisphere. These maps show the color variation across the surface from the very red terrain in the equatorial region, to the more neutral colors of the volatile ices in Sputnik Planitia, the blue terrain of East Tombaugh Regio, and the yellow hue on Pluto's North Pole. There are two distinct color mixing lines in the color-color diagrams derived from images of Pluto. Both mixing lines have an apparent starting point in common: the relatively neutral-color volatile-ice covered terrain. One line extends to the dark red terrain exemplified by Cthulhu Regio and the other extends to the yellow hue in the northern latitudes. There is a latitudinal dependence of the predominant color mixing line with the most red terrain located near the equator, less red distributed at mid-latitudes and more neutral terrain at the North Pole. This is consistent with the seasonal cycle controlling the distribution of colors on Pluto. Additionally, the red color is consistent with tholins. The yellow terrain (in the false color images) located at the northern latitudes occurs at higher elevations.

Key words: Kuiper belt objects: individual (Pluto) – planets and satellites: surfaces

1. Introduction

Investigations of Pluto's color at visible wavelengths have progressed from color photometry of the combined light of Pluto and Charon, to color maps from the mutual transits and occultation of Pluto and Charon (Binzel 1988; Young et al. 2001), to *Hubble Space Telescope* observations in different passbands resulting in maps (Buie et al. 2010). In 2015, *New Horizons* provided the first high-resolution color imaging of Pluto (Stern et al. 2015). This paper describes the color of Pluto from the highest resolution color images recorded by the spacecraft.

The color images were taken with the Ralph instrument (Reuter et al. 2008), which has two focal planes: (1) the Multi-spectral Visible Imaging Camera (MVIC) and (2) the Linear Etalon Imaging Spectral Array (LEISA). A single telescope with a beamsplitter (at 1.1 μm) sends light to each of the focal planes. MVIC has seven separate detectors, six time-delay integration (TDI) CCDs, and one frame transfer CCD. Four of the TDI CCDs are used for color observations; the other focal planes provide panchromatic imaging capabilities. When a color observation is executed, *New Horizons* data are recorded

from all four color TDI arrays simultaneously. Each TDI array has 32×5000 optically active pixels (Reuter et al. 2008). There are three broadband channels: blue, red, near-infrared, and a narrow band methane channel (Table 1). The narrow band channel is called the methane channel because it is sensitive to methane ice absorptions at 890 nm. The responsivity of each of the MVIC channels is described in Howett et al. (2017).

2. Observations

The *New Horizons* mission began observing Pluto in color in 2015 April, more than three months before the closest approach to Pluto. The observations from 2015 April to mid June did not resolve the disk of Pluto, but they did provide global color of Pluto over multiple rotations at a unique phase angle (15°) not obtainable from Earth. This paper focuses on the 17 color images taken with MVIC within the last approximately 5.5 days on approach to Pluto (see Table 2). Each line in the table describes an observation that is a single MVIC TDI scan that covered Pluto. Most of these observations additionally included Charon and some observed Nix

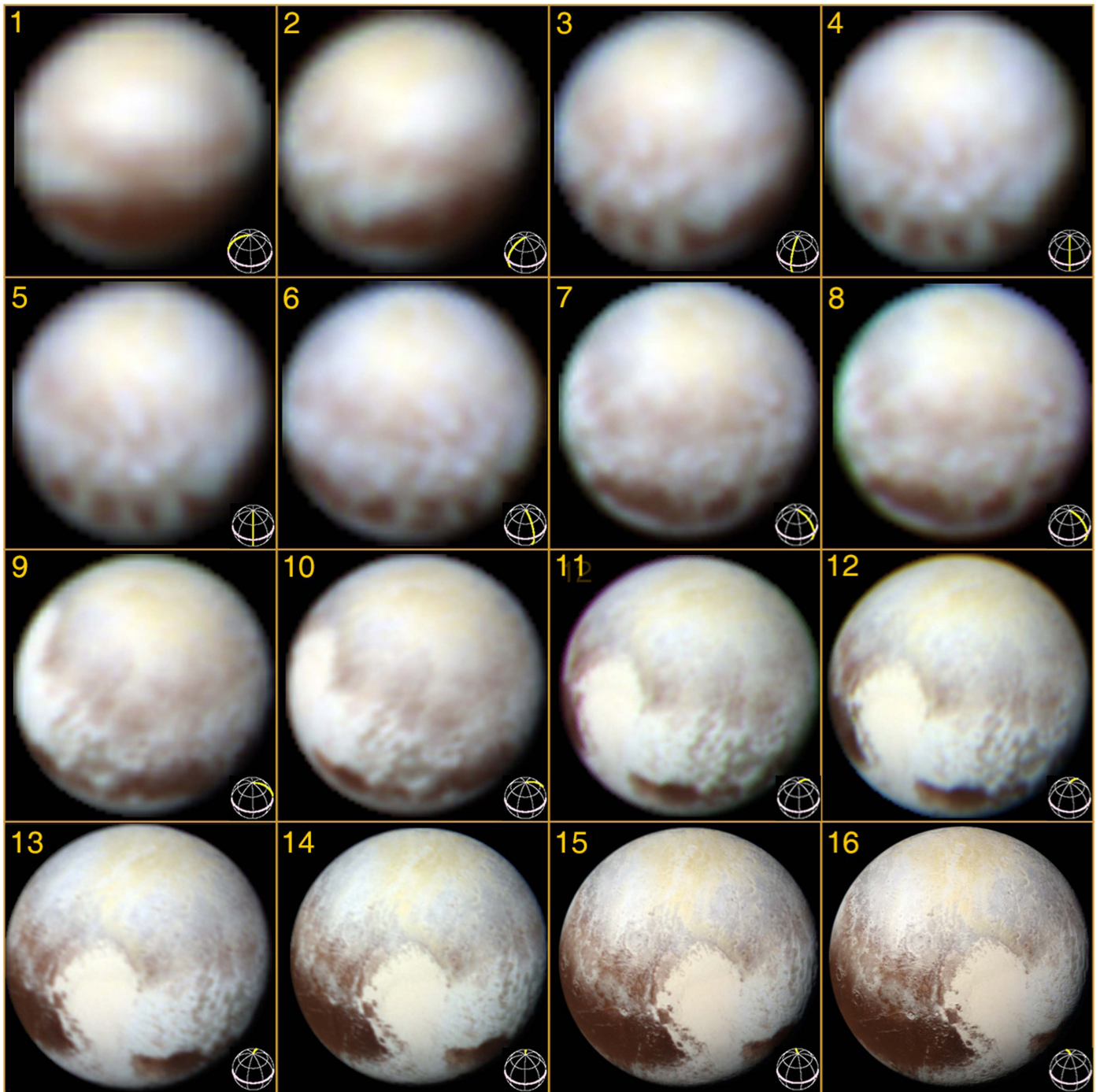


Figure 1. A mosaic of 16 Pluto images from *New Horizons*. The first image (PEMV_01_PC_MULTI_MAP_B_5) is at the upper left; read from left to right and top to bottom. The spatial resolution of the images improves from upper left to lower right because each successive image was taken at a closer range to Pluto than the previous one. The lower right image is PEMV_01_PC_COLOR_1. These images are enhanced color and do not represent the color of Pluto as it would be seen by the human eye. These images are produced using the I/F of the blue, red, and NIR observations, which are displayed in the blue, green, and red color channels, respectively. The geometry of the image is depicted by a wiregrid globe with the equator highlighted in pink and the prime meridian indicated in yellow.

Table 1
Filter Passbands

Filter	Wavelength Range, nm
Blue	400–550
Red	540–700
Near-infrared (NIR)	780–975
Methane	860–910

and Hydra as well. Other papers by Howett et al. (2017) and Grundy et al. (2016) describe the color of Charon and a mechanism to explain its red North Pole. The colors of the small satellites have been discussed in Weaver et al. (2016).

The Request ID in Table 2 is an identifier of the observation used in planning the observing sequence. The first four letters PEMV stand for Pluto Encounter MVIC observation. The next two digits are the visit number, which indicate if this is a



Figure 2. The highest resolution color image of Pluto from *New Horizons* (PEMV_01_P_COLOR2). At the sub-spacecraft point, a pixel subtends ~ 660 m. Detailed color variation across Pluto is evident from the dark red terrain that dominates the equatorial regions, the relatively blue hues across eastern Tombaugh Regio and the yellow coloration at the North Pole.

repeated observation (note that two of the observations are repeated to give increased observations of a particular longitude). The next letter sequence gives the intended targets of the observation: PC stands for Pluto and Charon, and PCNH stands for Pluto, Charon, Nix and Hydra. The remainder of the Request ID indicates the purpose for the observation: mapping, time resolution, or color imaging. The Mission Elapsed Time (MET) in the table is a counter on the spacecraft that increments each second since launch and provides a unique timestamp for the data. The image scale on the surface of Pluto ranges from 127 km/pix to 660 m/pix across this data set. The Ralph electronics side used for each observation is given in the last column of Table 2. The Ralph instrument has redundant

electronics that are denoted Side 0 and Side 1. To provide redundancy in our observation planning, we generally alternated which electronics side was powering the instrument for each observation.

The first 16 observations in Table 2 are displayed in Figure 1 and the last observation in the table is shown separately in Figure 2 because it is the highest resolution color image of Pluto. These images are enhanced color (not natural color as perceived by the human eye) using the three broadband filters of MVIC. The changing sub-spacecraft longitude over this sequence of images is due to the rotation of Pluto about its spin axis, which has a period of approximately 6.4 days. This sequence of observations covers about 280° of sub-spacecraft

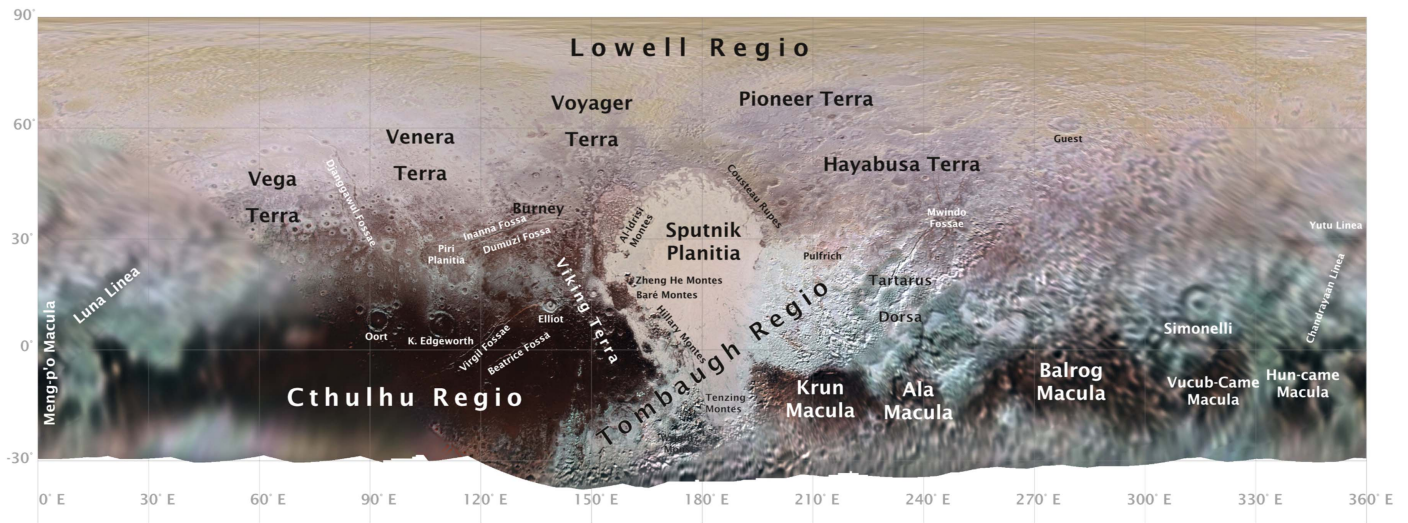


Figure 3. A color map of Pluto’s surface with a combination of formal and informal feature names indicated. This is a mosaic of the color images with a different color stretch than in Figures 1 and 2.

Table 2
Color Observations of Pluto

Request ID	Mid-time of Observation (UTC)	MET (s)	Image Scale (km/pix)	Sub-s/c Long. (Deg E)	Sub-s/c Lat. (Deg N)	Electronics Side	
1	PEMV_01_PC_MULTI_MAP_B_5	2015 Jul 09T03:41:05.936	298719178	127.16	87.4	43.1	0
2	PEMV_01_PC_MULTI_MAP_B_6	2015 Jul 09T16:56:05.937	298766878	114.03	56.3	43.1	1
3	PEMV_01_PC_MULTI_MAP_B_8	2015 Jul 10T08:55:30.937	298824443	98.17	18.8	43.0	0
4	PEMV_01_PC_MULTI_MAP_B_9	2015 Jul 10T16:52:15.938	298853048	90.28	0.2	43.0	1
5	PEMV_02_PC_MULTI_MAP_B_9	2015 Jul 10T16:55:05.938	298853218	90.24	0.0	43.0	1
6	PEMV_01_PC_MULTI_MAP_B_11	2015 Jul 11T03:34:35.938	298891588	79.66	335.1	43.0	0
7	PEMV_01_PC_MULTI_MAP_B_12	2015 Jul 11T16:46:56.439	298939128	66.54	304.1	43.0	1
8	PEMV_02_PC_MULTI_MAP_B_12	2015 Jul 11T16:49:46.439	298939298	66.49	304.0	43.0	1
9	PEMV_01_PC_MULTI_MAP_B_14	2015 Jul 12T08:23:08.440	298995300	51.03	267.6	43.0	0
10	PEMV_01_PC_MULTI_MAP_B_15	2015 Jul 12T16:53:04.940	299025878	42.59	247.7	42.9	1
11	PEMV_01_PC_MULTI_MAP_B_17	2015 Jul 13T03:38:06.440	299064598	31.91	222.6	42.9	0
12	PEMV_01_PC_MULTI_MAP_B_18	2015 Jul 13T07:38:36.941	299079028	27.93	213.2	42.8	1
13	PEMV_01_PC_MULTI_LONG_1d1	2015 Jul 13T14:50:51.941	299104958	20.78	196.5	42.7	0
14	PEMV_01_PC_MULTI_LONG_1d2	2015 Jul 13T21:08:40.941	299127628	14.53	182.1	42.5	1
15	PEMV_01_PC_COLOR_TIMERES	2015 Jul 14T02:47:54.441	299147983	8.92	169.5	42.1	0
16	PEMV_01_PC_COLOR_1	2015 Jul 14T06:50:11.942	299162518	4.91	161.4	41.1	1
17	PEMV_01_P_COLOR2	2015 Jul 14T11:10:52.442	299178098	0.66	168.0	26.0	1

Table 3
Bias Levels

Filter	Bias, DN Electronics Side 0	Bias, DN Electronics Side 1
Blue	24	23
Red	25	23
Near-infrared (NIR)	25	24
Methane	24	24

longitude. The dark area at the bottom of the first image (PEMV_01_PC_MULTI_MAP_B_5) is Cthulhu Regio (some Pluto surface feature names are informal and others are formal), which can also be seen at the lower left in the highest resolution images. A color map of Pluto with latitude and longitude markings and feature names is provided in Figure 3. The color stretch of the Pluto map (Figure 3) was chosen to enhance the color differences across different color units and is different

from the color stretch of Figures 1 and 2, which simply used the I/F from the blue, red, and NIR observations in the blue, green, and red color channels.

3. Reduction

The raw images from the spacecraft were processed using the following steps.

1. The raw images have a bias level subtracted from the raw counts. The bias level is a fixed number that depends on the focal plane array and electronics side used for the observation and is given in Table 3.
2. Each row of the image is divided by a one-dimensional flat-field array (5000 elements long) to remove flat-field effects. The bias subtracted and flat-fielded images are archived on the Planetary Data Systems Small Bodies Node.

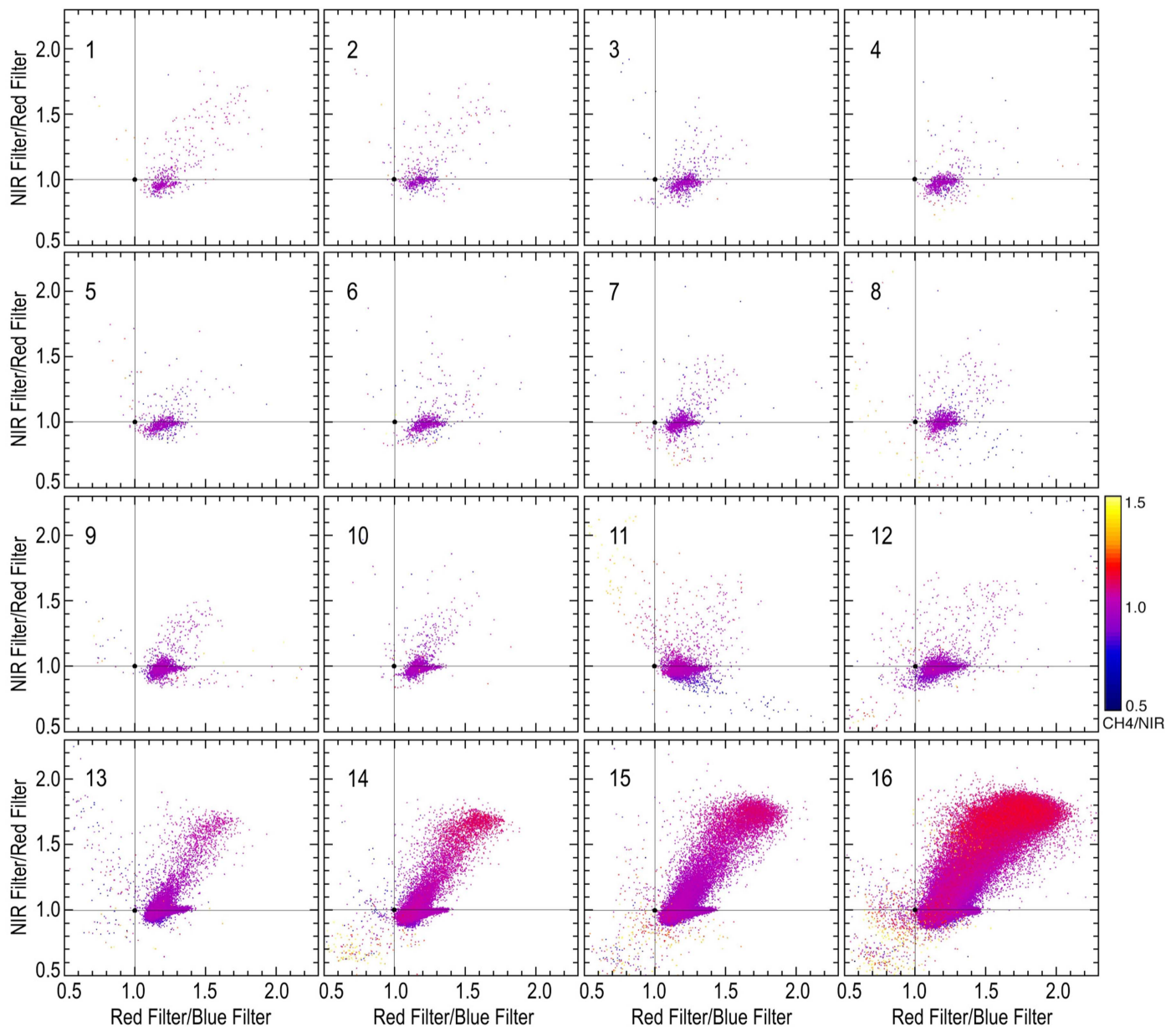


Figure 4. The color–color plots from 16 Pluto images. The color–color plots correspond to the images in Figure 1. For each pixel in the image, color ratios are plotted (NIR/red vs. red/blue). The neutral-color point is indicated by the black circle at the intersection of the lines. In the upper left of each panel is the line number from Table 2. The color of each point represents the ratio of I/F in the methane channel to the I/F in the NIR channel. Blue indicates more methane.

Table 4
Gain Correction Factors

Request ID	MET	Gain Factor from Charon	Gain Factor from Pluto	Electronics Side	
2	PEMV_01_PC_MULTI_MAP_B_6	298766878	0.917	0.909	1
4	PEMV_01_PC_MULTI_MAP_B_9	298853048	0.929	0.930	1
5	PEMV_02_PC_MULTI_MAP_B_9	298853218	0.956	0.963	1
7	PEMV_01_PC_MULTI_MAP_B_12	298939128	0.922	0.910	1
8	PEMV_02_PC_MULTI_MAP_B_12	298939298	0.954	0.940	1
10	PEMV_01_PC_MULTI_MAP_B_15	299025878	0.922	0.908	1
12	PEMV_01_PC_MULTI_MAP_B_18	299079028	0.919	0.905	1
14	PEMV_01_PC_MULTI_LONG_1d2	299127628	0.945	0.952	1
16	PEMV_01_PC_COLOR_1	299162518	1.036	1.048	1
17	PEMV_01_P_COLOR2	299178098	N/A	0.960	1

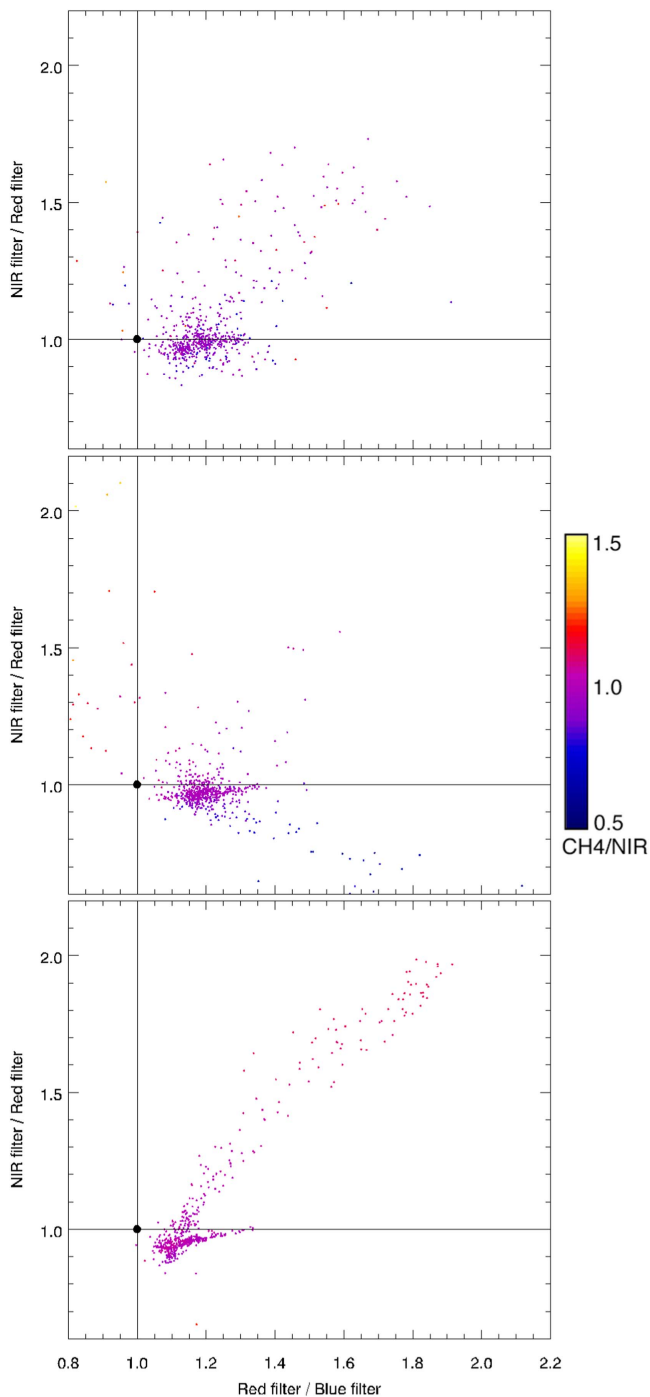


Figure 5. Color-color plots for three Pluto observations separated by 120° of longitude binned to the same resolution. The three observations from top to bottom are PEMV_01_PC_MULTI_MAP_B_6, PEMV_01_PC_MULTI_MAP_B_17, and PEMV_01_P_COLOR2.

3. Model and remove the low-level (approximately 2 DN) pattern noise. The noise has a striped pattern that aligns with the row direction of the detector locally, but it is not consistent across the whole field of view. Using the pixels adjacent to the Pluto image, a model for the pattern noise can be determined and removed. Note that Pluto is typically between 20 and 700 DN in blue images and brighter in the other broadband filters (red and NIR), so the pattern noise is a small fraction of the total signal.

4. Convert the signal from DN to I/F using the method described in Howett et al. (2017). There are different radiometric calibration keywords that could be used when converting to I/F that depend on the color of the terrain. For this analysis, we have used the RSOLAR keyword, which is an approximation.

MVICs four color CCDs are adjacent to one another on the focal plane, and thus they do not image the same field of view. Through scanning, they cover the same field of view, but not simultaneously. At the usual scan rate of 1045 rad s^{-1} , it takes six seconds to sweep all four CCDs across a point in the target scene. The finite scan rate combines with spacecraft and target motion so that each of the MVIC colors images a point on the target from a slightly different point of view, so the geometry is a little different. Thus, each color channel is treated as an independent instrument and registered to the relevant Pluto and Charon base maps separately (Schenk et al. 2016). After they are all registered to the base map, they can be reprojected to a common geometry. To perform this task, we used version 3.5.0.7383 of the Integrated Software for Images and Spectrometers (ISIS3) package from the United States Geological Survey and selected the geometry for the BLUE filter as our target geometry for each scan. As this involves resampling, we sub-sampled to a finer grid approximately a factor of two finer than the original pixel scale to minimize loss of spatial information.

On approach to Pluto, we discovered that the gain of the NIR channel on the side 1 electronics is not consistent from observation to observation. The gain is consistent over a single image but varies from image to image at the 5%–10% level. For the first 16 images of Table 2, Charon appears in all of the images and could be used as a standard. The color of the terrains on Charon is longitudinally uniform and could be used to determine the gain offset using the Side 0 image taken before or after the Side 1 image with unknown gain. This was achieved by first computing and saving red/NIR and red/blue ratios for every Charon pixel in all Side 0 images on approach. An empirical model of the two-dimensional distribution of red/NIR and red/blue ratios for all Charon hemispheres is built by passing these Side 0 ratios through a Gaussian Kernel Density Estimator. Correction terms were found computing the red/NIR and red/blue ratios for the Charon pixels in any given Side 1 image, and finding a scaling factor on the Red/NIR ratio ($c_i \times \text{Red/NIR}$) that maximized the likelihood that this sample of ratios was drawn from the empirical model.

The highest resolution Pluto color image did not have Charon in the field of view; therefore, the same approach used deriving a Charon-based correction term was used, but with color ratios drawn instead from Pluto’s terrains. To determine the consistency of this approach, we calculated these Pluto-derived correction terms for all Side 1 color images in Table 2 to compare the results of this method to the Charon deduced adjustment factors for the gain. They demonstrate excellent consistency. The results are shown in Table 4.

4. Analysis

Each pixel in the resolved images of Pluto has a different incidence and emission angles. This initial analysis of Pluto color focuses on what we can learn from color ratios because

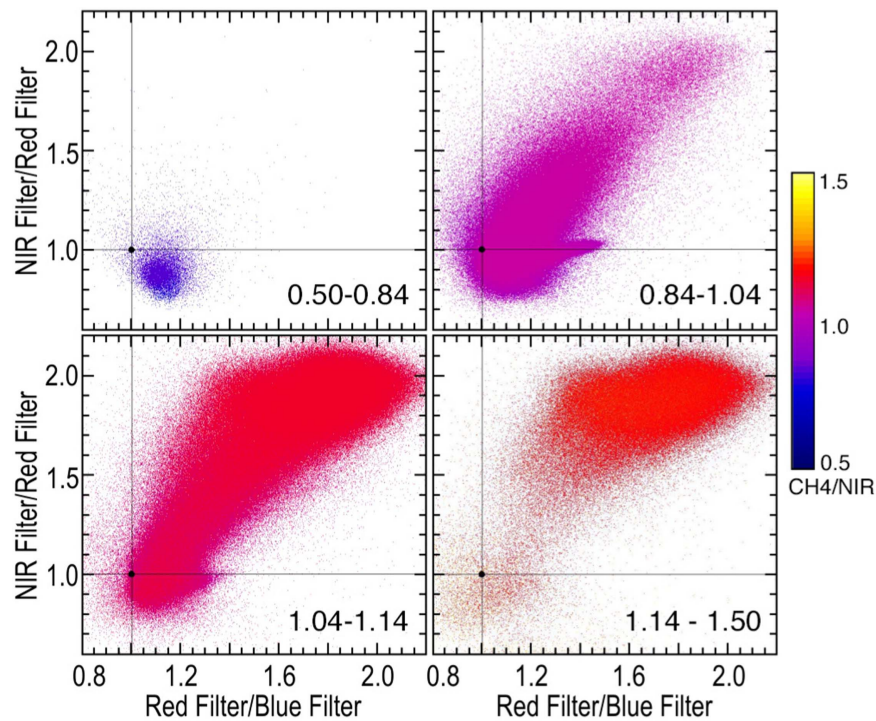


Figure 6. A mosaic of color-color plots for the highest resolution color image of Pluto. The color of each point represents the ratio of the I/F in the methane filter to the I/F in the NIR filter, as shown in the color bar. Blue points indicate a lower ratio for the I/F of methane to NIR, which is consistent with absorption by methane ice at 890 nm. Each panel is a color-color plot from the observation PEMV_01_P_COLOR2 displaying a different range of ratios for methane to NIR. Pixels that have the methane to NIR ratio in the range from 0.50 to 0.84 are displayed in the upper right. The panels increase in methane to NIR ratio from left to right and top to bottom.

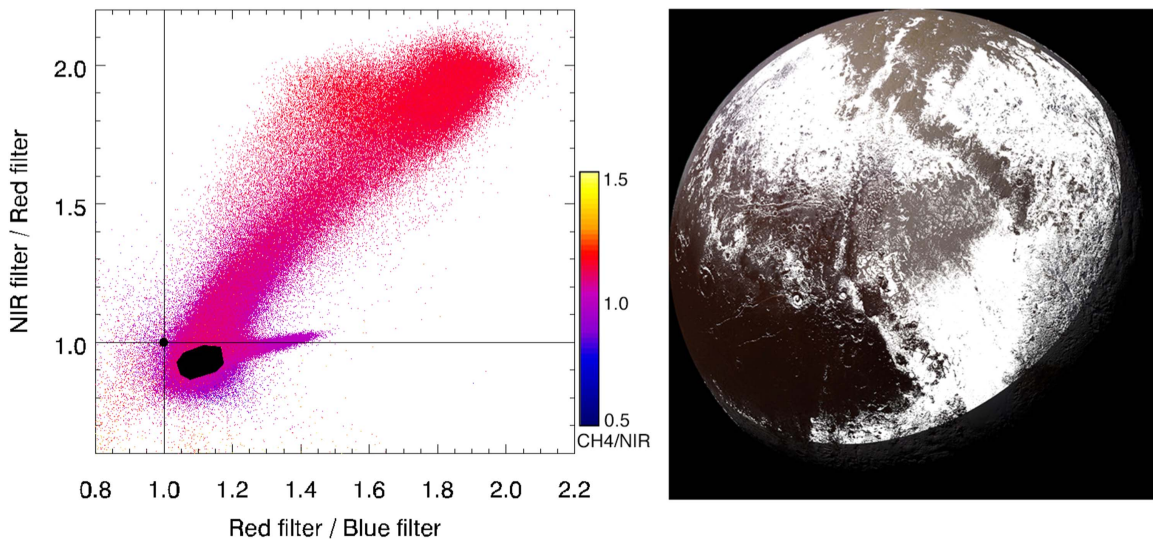


Figure 7. Left: the color-color diagram for PEMV_01_P_COLOR2 with selected pixels on the diagram indicated in black. Right: the PEMV_01_P_COLOR2 image with the selected pixels from the color-color diagram indicated in white. These pixels are representative of the neutral end member in the predominant color mixing line. The sharp edge at the lower right of the globe is a result of only considering pixels with an emission angle $< 80^\circ$.

the color ratio is less dependent on the directional scattering properties of the surface elements. Figure 4 displays the color-color diagrams for the first 16 Pluto images in Table 2. For each pixel in the image, the ratio of the NIR filter I/F to red filter I/F is plotted against the ratio of the red filter I/F to the blue filter I/F. Only pixels with an incidence and emission angle less than 80° are included in the diagrams.

Pixels that are more red from 400–700 nm fall to the right of the vertical line denoting a neutral red/blue ratio. Almost all

pixels across all Pluto terrains visible to New Horizons are red in the wavelength range of 400–700 nm. Pixels that are more red from 540 to 975 nm fall above the horizontal line denoting a neutral NIR/red ratio. The color of each point in the figure is the ratio of I/F in the methane channel to the I/F in the NIR channel.

While the terrain on the Charon-facing hemisphere of Pluto (panels 4 and 5 of Figure 4, sub-spacecraft longitude near 0°) has dark Maculae spanning the globe just south of the equator

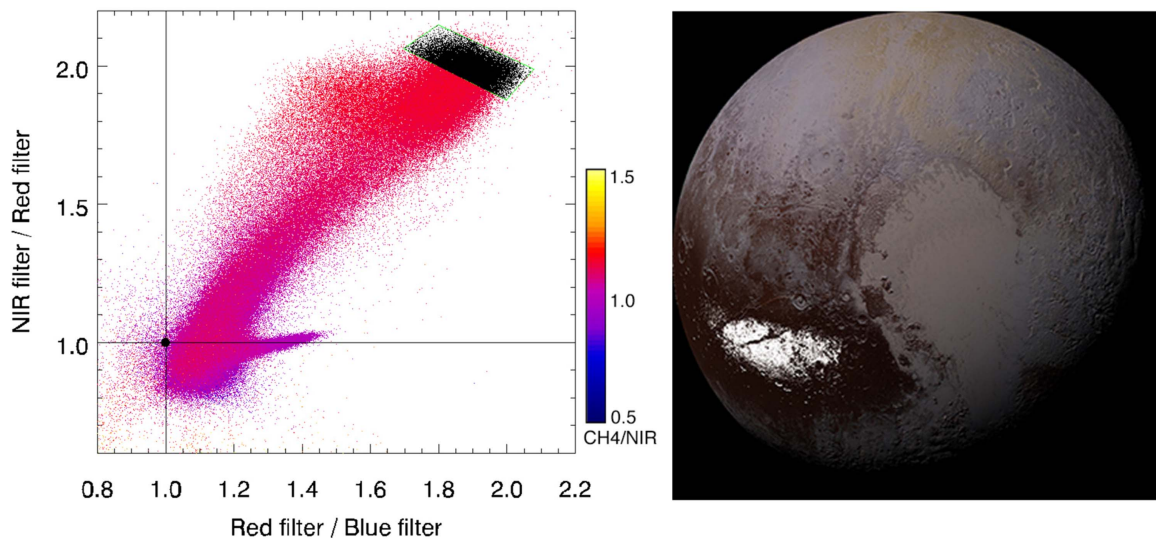


Figure 8. Left: the color–color diagram for PEMV_01_P_COLOR2 with selected pixels on the diagram indicated in black. Right: the PEMV_01_P_COLOR2 image with the selected pixels from the color–color diagram indicated in white. These are the most red terrain in the predominant color mixing line and correspond to the center of Cthulhu Regio.

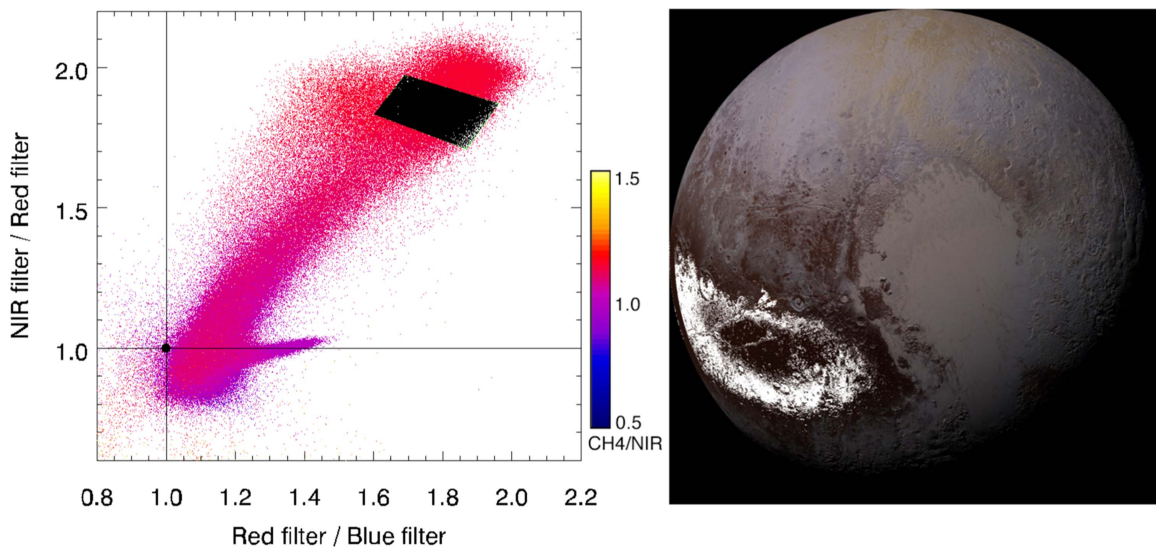


Figure 9. Left: the color–color diagram for PEMV_01_P_COLOR2 with selected pixels on the diagram indicated in black. Right: the PEMV_01_P_COLOR2 image with the selected pixels from the color–color diagram indicated in white. These are red regions that are less red than the center of Cthulhu Regio as indicated by their location on the color–color diagram and they encircle the center of CR.

(Meng-p’o, Hun-came, and Vucub-came Maculae), those terrains are less red than the reddest terrain in Cthulhu Regio. This can be seen by comparing the extent of the points in the color–color diagram across the 16 images. In panels 4 and 5, there are very few pixels (as a fraction of the total) with color ratios greater than 1.4 in both axes, compared to both panels 16 and 1. To explicitly remove the effect of different spatial resolution, Figure 5 shows a comparison of color–color plots from three different observations (separated by approximately 120° of longitude) after downsampling the later two observations to the spatial resolution of the first image. Comparing the color–color plots from these three observations shows that the encounter hemisphere (anti-Charon face of Pluto) has the most red terrain on Pluto with the NIR/red ratio reaching 2 and the

red/blue ratio reaching 1.8 even in the downsampled image. The western part of Cthulhu Regio is visible in observation PEMV_01_PC_MULTI_MAP_B_6, and this terrain is red, but as seen in Figure 5, the color is not as extreme as the red color seen in the non-Charon hemisphere of Pluto at closest approach.

The color–color plot for the highest resolution Pluto image is shown in Figure 6 with each panel displaying different values of the methane I/F to NIR I/F ratio, hereafter referred to as methane to NIR ratio. The terrain with the smallest ratio of methane/NIR likely have methane on the surface due to absorption by methane ice at 890 nm. These pixels are blue from 540–975 nm (below the horizontal line) and red from 400–700 nm (to the right of the vertical line). This corresponds

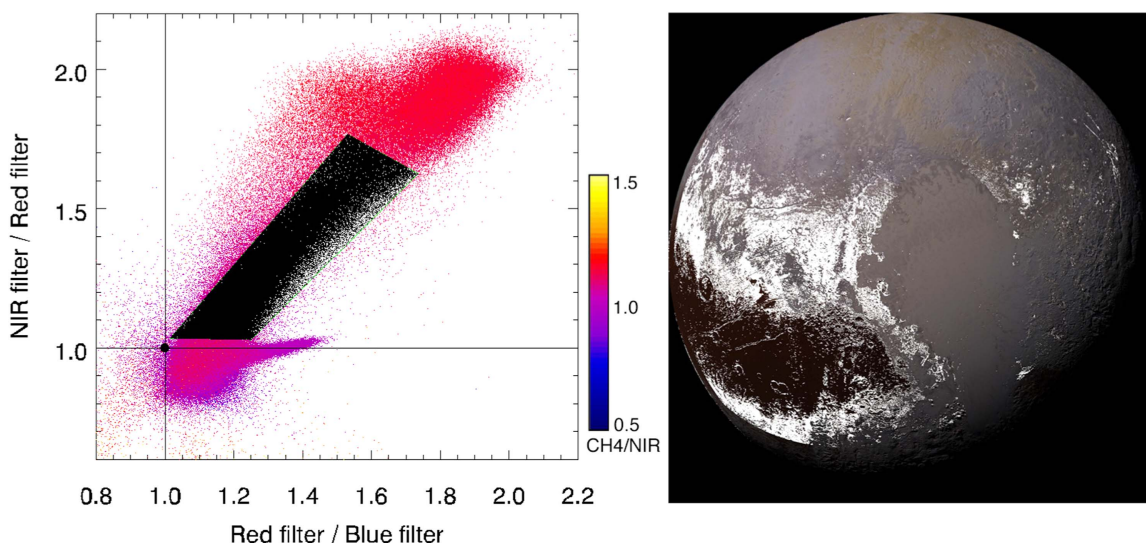


Figure 10. Left: the color-color diagram for PEMV_01_P_COLOR2 with selected pixels on the diagram indicated in black. Right: the PEMV_01_P_COLOR2 image with the selected pixels from the color-color diagram indicated in white. The transitional terrain between the red of Cthulhu Regio and the more neutral ices is found at mid-latitudes. This transitional terrain is also found in the low-elevations of Cthulhu Regio, as noted by the linear features across this area (corresponding to part of Virgil and Beatrice Fossae).

to the areas of central and south Sputnik Planitia (north Sputnik Planitia is more red) and the mid-latitudes, regions both known to be nitrogen-rich with small amounts (0.1% to 1%) of methane from LEISA infrared spectroscopy (Schmitt et al. 2017). In contrast, the color-color units with the highest methane/NIR ratio, which have no significant absorption at 890 nm, are located in the upper right of the color-color plot. This corresponds to the dark red near-equatorial regions.

There are what appears to be two distinct color mixing lines in the color-color plots. The steeper-sloped color mixing line comprises the bulk of the pixels on Pluto and the less-steep slope color mixing line corresponds to the yellow regions concentrated near Pluto’s North Pole.

First we consider the steep-sloped mixing line. The end members of this color mixing line are the high albedo icy terrain (Figure 7) and the dark red terrains of Cthulhu Regio (see Figures 8 and 9). The intermediate pixels along the primary color mixing line correspond to the less red terrain to the north and south of Cthulhu Regio, see Figure 10. For each of these figures, the globe and color-color diagram have been constructed from the image after binning over 3×3 pixel boxes.

As shown in Figure 7, the more neutral-color end member spans southern Sputnik Planitia, the mid-latitude icy terrains, and the valley extending into Pluto’s North Pole. The red end of this color mixing ratio is the central region of Cthulhu Regio (Figure 8). The concentric region around the center of Cthulhu Regio has a location along this mixing line abutting the most red terrain (Figure 9). The color of the red terrain is consistent with the presence of tholins as inferred from infrared spectroscopy of Pluto from New Horizons (Protopapa et al. 2017). While tholins can exhibit different colors depending on the initial composition and the irradiation history, they are typically a dark red. Using the reflectivity of an Ice Tholin sample (Cruikshank et al. 2016), we computed the I/F color ratios for red/blue to be $2.49^{+1.00}_{-0.61}$ and for NIR/red to be $2.25^{+0.31}_{-0.28}$, and these values are consistent with the red end member of the steep-sloped mixing line. The error estimates for the color ratios of the

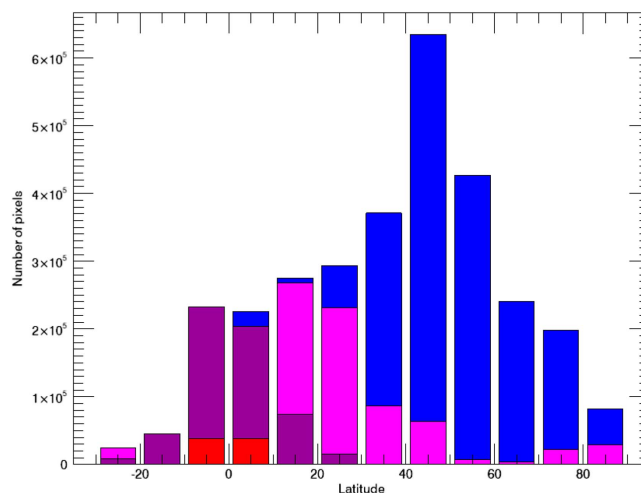


Figure 11. A histogram of the number of pixels from the observation PEMV_01_P_COLOR2 with a range of color ratios (NIR/red) as a function of latitude. Red indicates $\text{NIR/red} \geq 2$; purple is $1.5 \leq \text{NIR/red} < 2$; pink is $1.0 \leq \text{NIR/red} < 1.5$; blue is $\text{NIR/red} < 1$.

laboratory samples were constructed from the uncertainty in reflectivity of Ice Tholin.

The distribution of the red terrain is likely the result of Pluto’s insolation cycle at seasonal and longer timescales. This region never experiences darkness through a full Pluto rotation at any point in Pluto’s precessional cycle, thus plausibly reducing the opportunity for deposition of volatile ices (nitrogen, methane, and carbon monoxide) at that latitude (Binzel et al. 2017). The color gradient across Cthulhu Regio is consistent with the idea of seasonal insolation gradients causing the color variation because the most red terrain is located nearest to the equator. Figure 11 shows a histogram of the color ratio (NIR/red) for the pixels of PEMV_01_P_COLOR2 as a function of latitude. For this figure, the pixels below -2 km elevation were excluded to remove the pixels from Sputnik Planitia (SP). SP is a basin and volatile ices condense preferentially in the basin (Bertrand & Forget 2016).

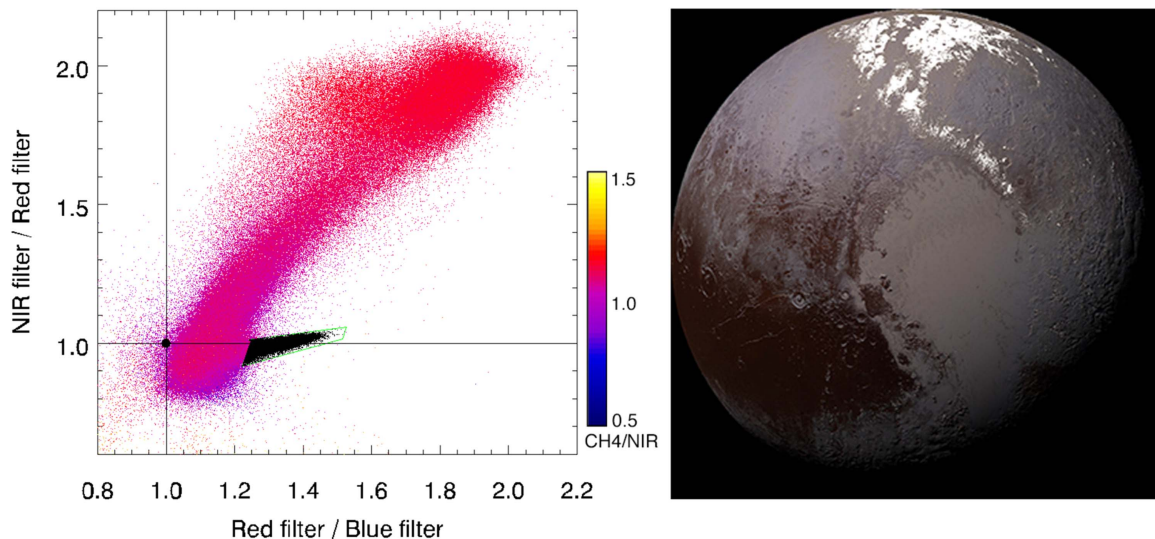


Figure 12. Left: the color-color diagram for PEMV_01_P_COLOR2 with selected pixels on the diagram indicated in black. Right: the PEMV_01_P_COLOR2 image with the selected pixels from the color-color diagram indicated in white. This yellow terrain is located near Pluto’s North Pole. The selected pixels fall on the less-steep-sloped color mixing line.

The basin disrupts the general trend of color with latitude and is therefore excluded from the histogram in Figure 11. The most red terrain (indicated by red in the histogram and corresponding to an NIR/red ratio > 2) only occurs near the equator; the next most red terrain (indicated in pink and with an NIR/red ratio between 1.5 and 2.0) is also found predominantly near the equator.

Next, we consider the less-steep color mixing line. Figure 12 shows selected points on this mixing line and the corresponding points on the color image. This terrain is associated with a yellow color near Pluto’s North Pole that extends southward to the northeast margin of SP. This color mixing line is evident in all of the color-color plots of Figure 4 because the North Pole of Pluto is visible in all of these images.

The yellow coloring agent is likely distinct from the dark red coloring agent that dominates Pluto’s surface because of the distinct population of pixels on the two color mixing lines. This yellow color unit is generally associated with higher elevation terrain (discussed more below). This color unit is correlated not only with high elevations, but also with a high fractional abundance of $\text{CH}_4:\text{N}_2$ and a reduced fractional abundance of $\text{N}_2:\text{CH}_4$ ($< 20\%$) as shown in Figure 13 (Protopapa et al. 2017). The solid solution of CH_4 and N_2 can exist in a CH_4 -rich state ($\text{CH}_4:\text{N}_2$) or in a N_2 -rich state ($\text{N}_2:\text{CH}_4$; Protopapa et al. 2015).

The yellow coloring agent could be a photolysis product from different molecular reactants than the dark red products seen at more equatorial latitudes. Specifically, the North Pole region is depleted in nitrogen compared to more mid-latitudes, which show a combination of volatile ices including nitrogen and dark red materials. If the yellow material formed in place, it would require an energy source for the photolysis such as UV radiation or cosmic rays. At current atmospheric pressures, no significant UV radiation reaches the surface for photolysis to be an active process. Further analysis is needed to understand if photolysis could occur on the surface through UV solar radiation during periods of rarefied atmosphere or if cosmic rays could provide sufficient energy.

There is an unusual red color unit associated with low-latitude troughs. The most prominent example of this color

unit is Virgil Fossa, but it can also be seen in Beatrice Fossa and another linear feature that is likely a topographic low, see the elevation map in the lower right panel of Figure 14. Note that the unusual red material is not present across all of Virgil or Beatrice Fossae, but it is localized in regions of these features, and the regions where the unusual red material is present correspond to the presence of water ice (Schmitt et al. 2017). Not everywhere that has water exhibits this unusual red color, but in all of these locations there is a combination of water and significant amounts of tholin.

Using a digital elevation map based on stereoscopic images from *New Horizons* (Schenk et al. 2016), the color of Pluto as a function of elevation can be examined. Figure 15 gives the color ratios for all pixels with incidence and emission angles less than 80° for PEMV_01_P_COLOR2 (unbinned). The color of the pixels represents the elevation of each surface element, ranging from -5 km to $+4$ km. To see the details of the color ratios with elevation, color-color diagrams for each one-km step in elevation are shown in Figure 16.

The lowest elevation terrain (in the top two panels of Figure 16) is that of SP. The less-steep color mixing line is not evident until the elevation is more than -2 km. For the highest elevation points, from $+2$ to $+3$ km elevation, the most dense region on the color-color diagram is the color mixing ratio corresponding to the yellow terrain.

There is a blue terrain that is most predominantly seen in the East Tombaugh Regio. This terrain is characterized by the presence of methane and a bluish color with color ratios: NIR/red < 0.97 , red/blue < 1.15 , and $\text{CH}_4/\text{NIR} < 0.92$. This blue terrain is also present at other longitudes just north of the equator in Figure 17.

5. Conclusions

There is large variegation across Pluto’s surface from the relatively blue terrain of the East Tombaugh Regio to the red of the Cthulhu Regio and the yellow of the North Pole. There is a general pattern of dark red material near the equator and bright, more neutral-colored materials near the pole, consistent with a volatile transport away from the equatorial regions that receive

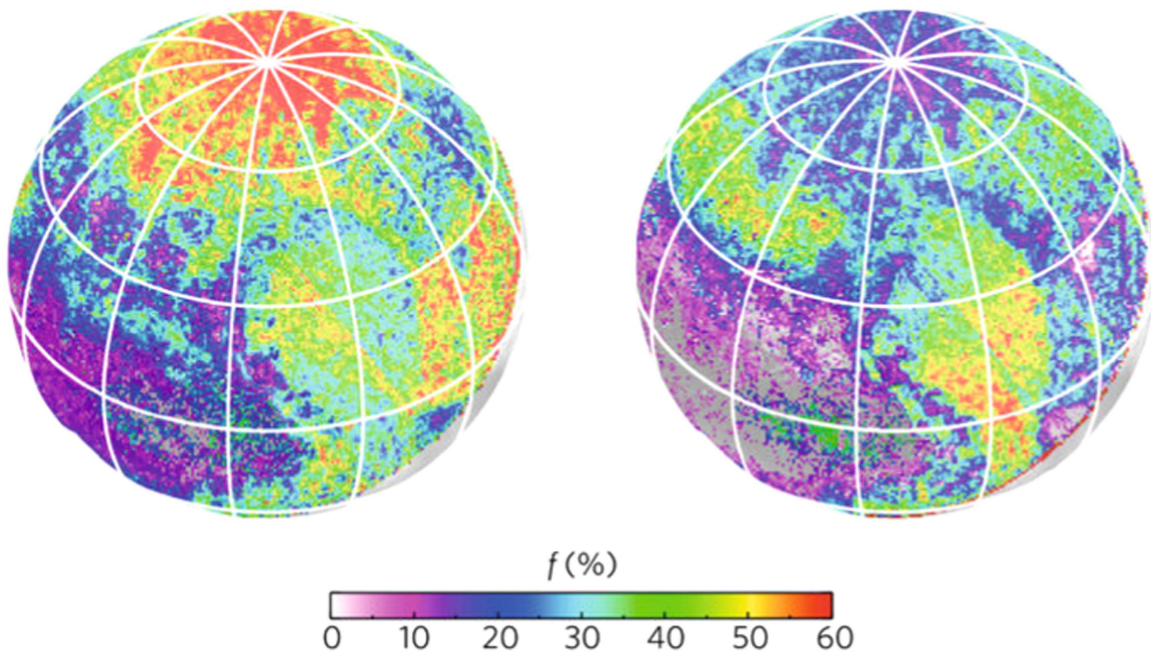


Figure 13. The fractional abundance of the solid solution of CH₄ and N₂ from Protopapa et al. (2015). Left: the fractional abundance of the CH₄-rich state. Right: the fractional abundance of the N₂-rich state. The location of the yellow terrain coincides with the location of the CH₄-rich state of the solid solution of CH₄ and N₂.

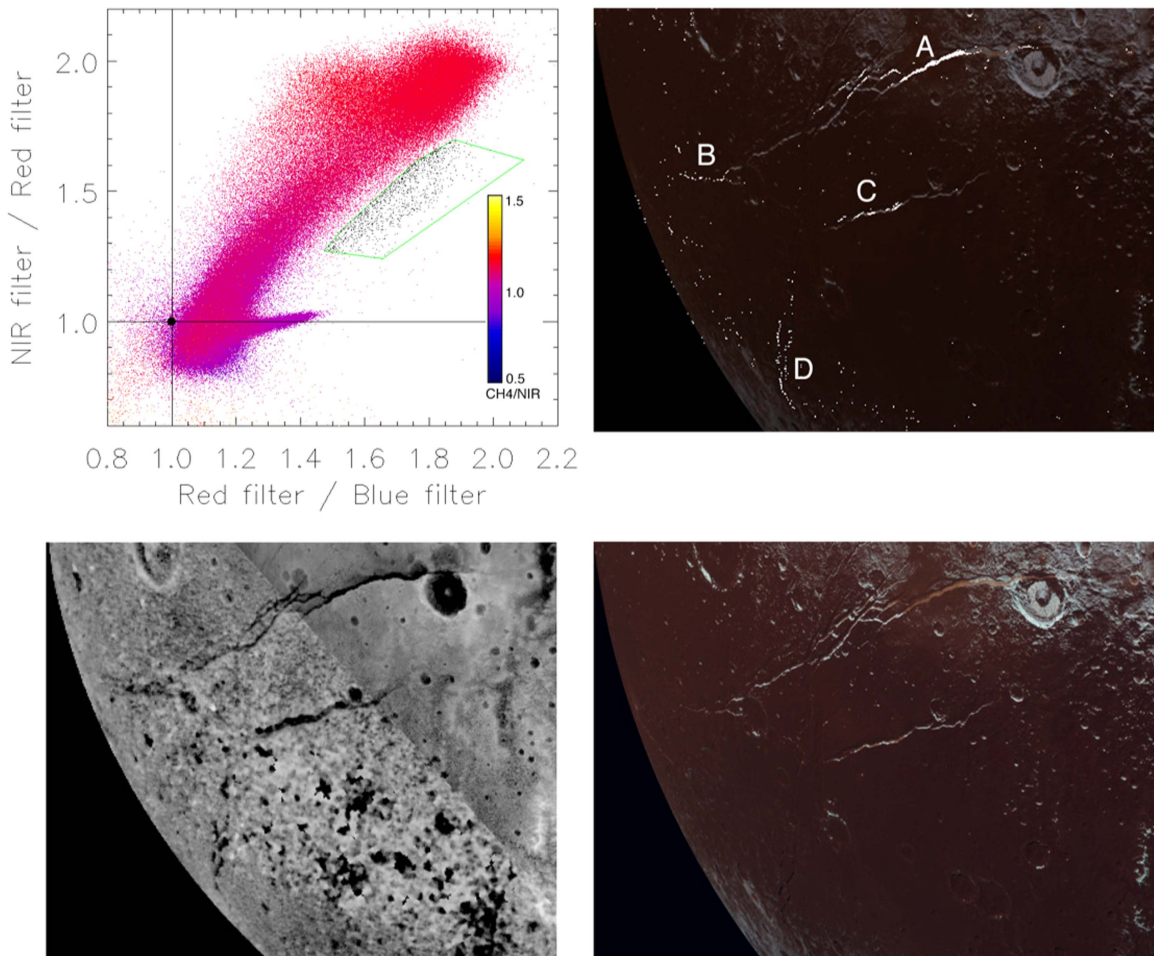


Figure 14. Top left: the color–color diagram for PEMV_01_P_COLOR2 with selected pixels on the diagram indicated in black. Top right: the PEMV_01_P_COLOR2 image with the selected pixels from the color–color diagram indicated in white. This unique red color is predominantly found in the Fossae in this region on Pluto: (A and B) Virgil Fossae, (C) Beatrice Fossa, and (D) another linear topographic low feature. Lower left: topographic map of the region (Schenk et al. 2016); the terrain varies from -1.5 km to 2 km in elevation (dark is low elevation). Lower right: the enhanced color image of this region from PEMV_01_P_COLOR2.

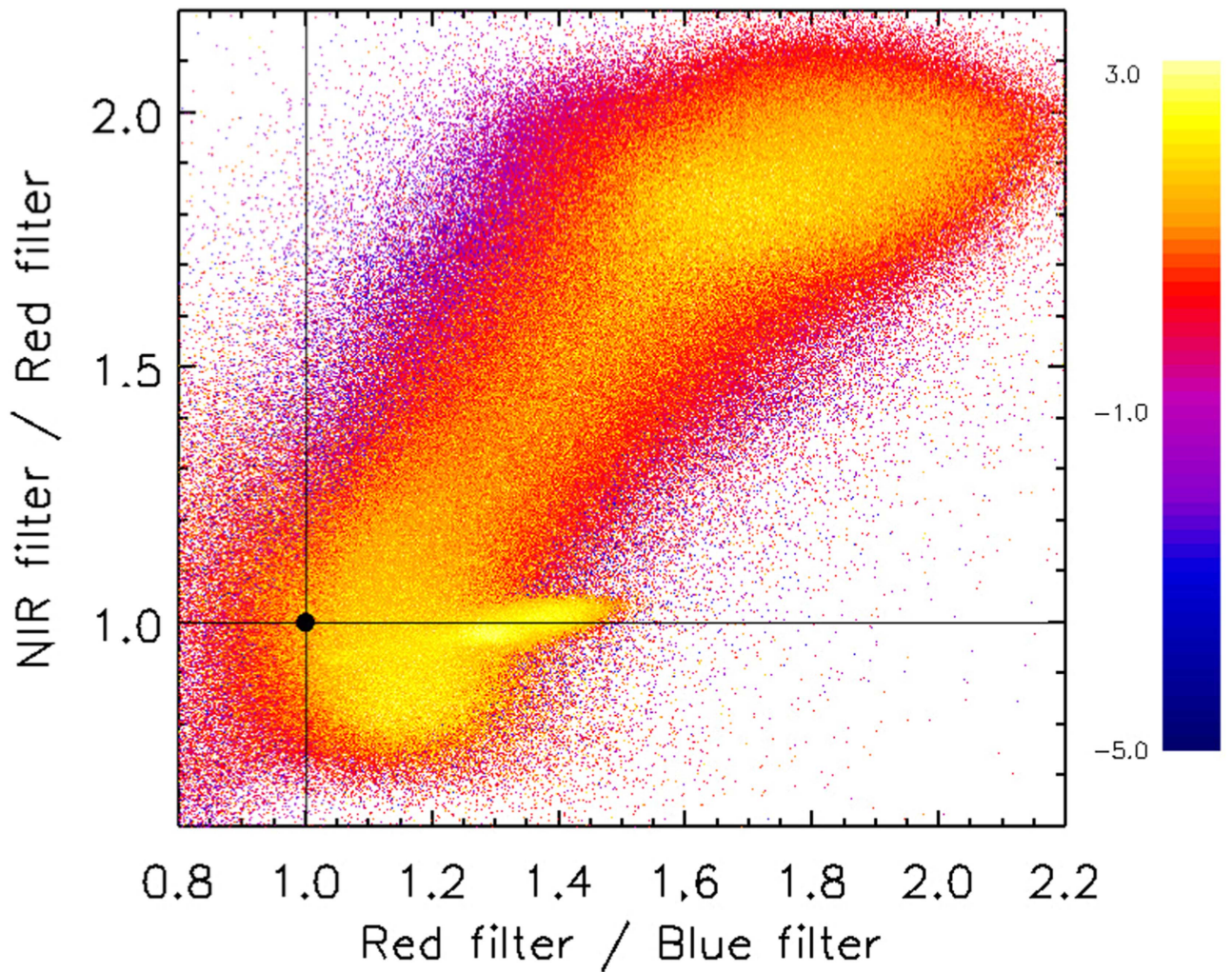


Figure 15. Color ratios of pixels on the highest resolution Pluto image with each point color coded for elevation, as given in the color bar. The elevation ranges from -5 km to $+3$ km.

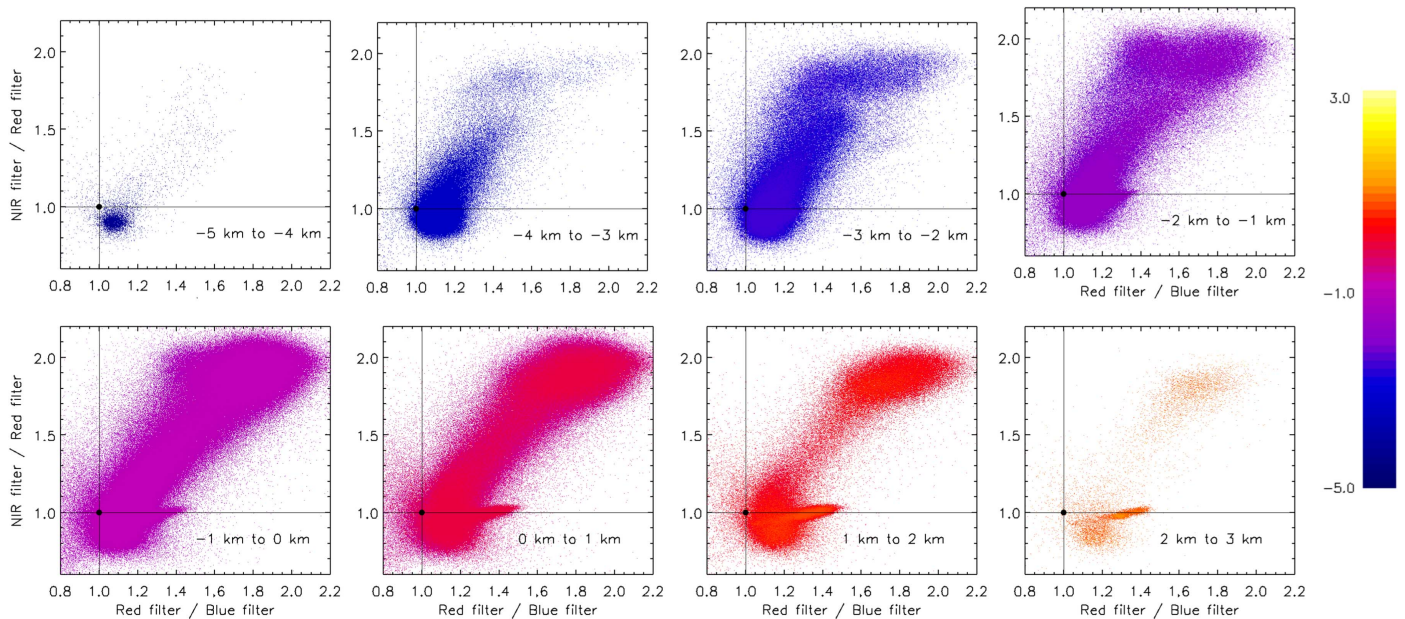


Figure 16. Color ratios of PEMV_01_P_COLOR2 as a function of elevation. The color ratios of Pluto terrain for 1-km bins in elevation are shown. The lowest elevation from -5 to -4 km is displayed in the upper left. The highest elevation from 2 to 3 km is displayed in the lower right. The same color scale is used as in Figure 15.

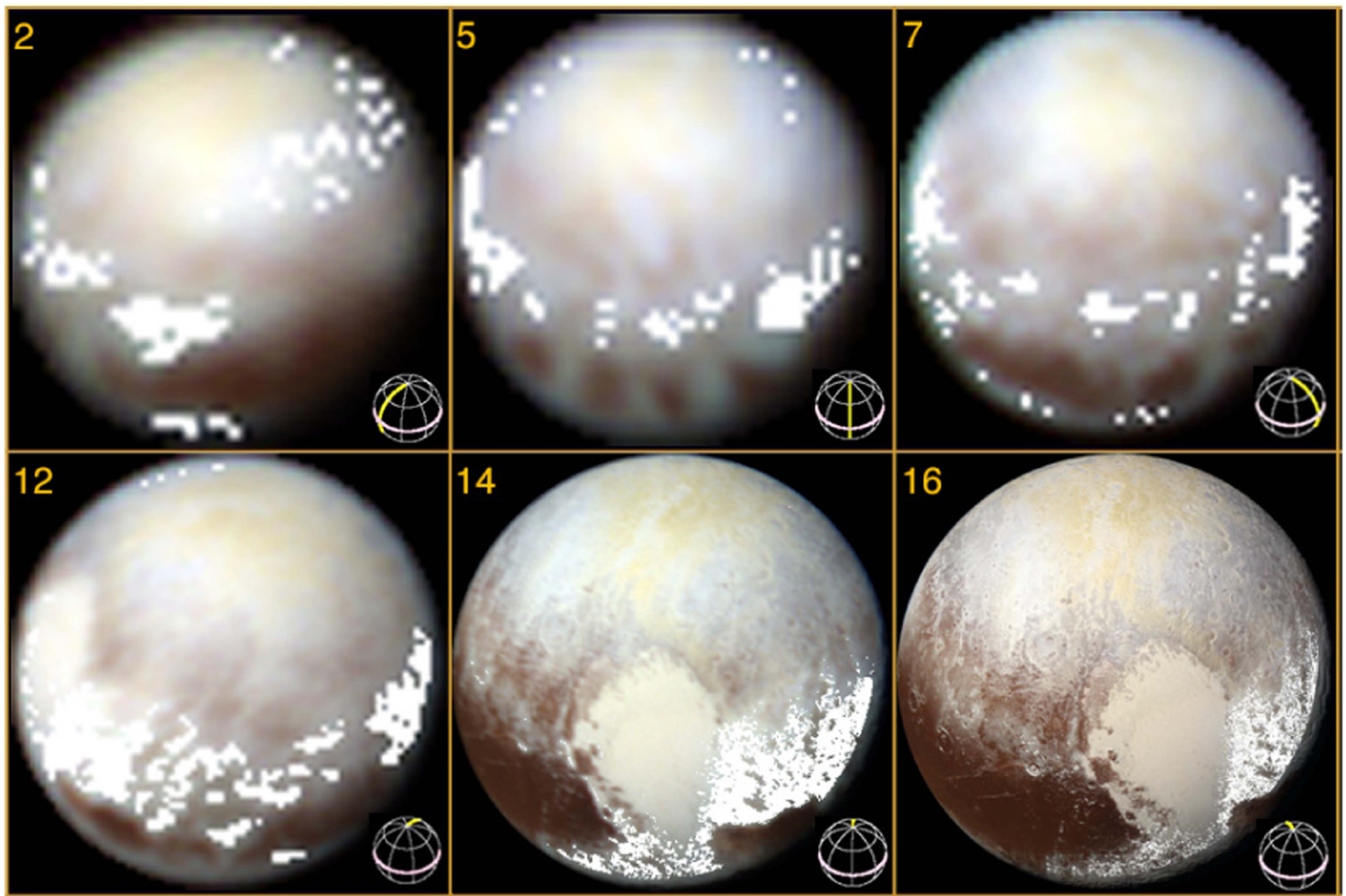


Figure 17. Selected images of Pluto with blue terrain indicated in white. The blue terrain is evident at different longitudes on Pluto north of the equator.

more insolation on a seasonal timescale than the poles (Binzel et al. 2017).

Distinct color units correlate with certain topographic features such as the yellow terrain located at high latitudes and high altitudes. Another example is the unusual red terrain located at or near the equator and along troughs.

Pluto passed through equinox in 1989 and will reach northern solstice in 2029, with the next equinox in 2110. For approximately the next 100 years, Pluto's icy North Pole will be in sunlight. Near northern solstice, it will be useful to observe the color of Pluto's North Pole and compare to these observations to look for a change in the overall color of Pluto's North Pole. This could constrain timescales for the processes affecting the color of Pluto's surface, particularly the yellow unit at the North Pole.

The authors gratefully acknowledge the support of NASA's New Horizons project.

ORCID iDs

Catherine B. Olkin <https://orcid.org/0000-0002-5846-716X>
 Alex H. Parker <https://orcid.org/0000-0002-6722-0994>
 Harold A. Weaver <https://orcid.org/0000-0003-0951-7762>

Kimberly Ennico <https://orcid.org/0000-0002-8847-8492>
 Marc W. Buie <https://orcid.org/0000-0003-0854-745X>
 Kelsi N. Singer <https://orcid.org/0000-0003-3045-8445>

References

- Bertrand, T., & Forget, F. 2016, *Natur*, 540, 86
 Binzel, R. P. 1988, *Sci*, 241, 1070
 Binzel, R. P., Earle, A. M., Buie, M. W., et al. 2017, *Icar*, 287, 30
 Buie, M. W., Grundy, W. M., Young, E. F., Young, L. A., & Stern, S. A. 2010, *AJ*, 139, 1128
 Cruikshank, D. P., Clemett, S. J., Grundy, W. M., et al. 2016, in LPSC, 1903, 1700
 Grundy, W. M., Cruikshank, D. P., Gladstone, G. R., et al. 2016, *Natur*, 539, 65
 Howett, C., Parker, A., Olkin, C., et al. 2017, *Icar*, 287, 140
 Protopapa, S., Grundy, W. M., Reuter, D. C., et al. 2017, *Icar*, 287, 218
 Protopapa, S., Grundy, W. M., Tegler, S. C., & Bergonio, J. M. 2015, *Icar*, 253, 179
 Reuter, D. C., Stern, S. A., Scherrer, J., et al. 2008, *SSRv*, 140, 129
 Schenk, P., Beyer, R. A., Moore, J. M., et al. 2016, AGUFM, P41C-03
 Schmitt, B., Philippe, S., Grundy, W. M., et al. 2017, *Icar*, 287, 229
 Stern, S. A., Bagenal, F., Ennico, K., et al. 2015, *Sci*, 350, aad1815
 Weaver, H. A., Buie, M. W., Buratti, B. J., et al. 2016, *Sci*, 351, aae0030
 Young, E. F., Binzel, R. P., & Crane, K. 2001, *AJ*, 121, 552